Initial Solvent-Driven Nonequilibrium Effect on Structure, Properties, and Dynamics of Polymer Nanocomposites

Sol Mi Oh,[1] Mozhdeh Abbasi,[3] Tae Joo Shin,[2] Kay Saalwächter,[3,†] and So Youn Kim[1,*]
[1]School of Energy and Chemical Engineering, Ulsan National Institute of Science and Technology (UNIST), 50 UNIST-gil Ulsan 44919, Republic of Korea
[2]UNIST Central Research Facilities & School of Natural Science, Ulsan National Institute of Science and Technology (UNIST), 50 UNIST-gil Ulsan 44919, Republic of Korea
[3]Institut für Physik-NMR, Martin-Luther-Universität Halle-Wittenberg, Betty-Heimann-Straβe 7, D-06120 Halle, Germany

(Received 24 June 2019; published 17 October 2019)

Unusual structures and dynamic properties found in polymer nanocomposites (PNCs) are often attributed to immobilized (adsorbed) polymers at nanoparticle-polymer interfaces, which are responsible for reducing the intrinsic incompatibility between nanoparticles and polymers in PNCs. Although tremendous effort has been made to characterize the presence of immobilized polymers, a systematic understanding of the structure and dynamics under different processing conditions is still lacking. Here, we report that the initial dispersing solvent, which is not present after producing PNCs, drives these nonequilibrium effects on polymer chain dynamics at interfaces. Employing extensive small-angle scattering, proton NMR spectroscopy, and rheometry experiments, we found that the thickness of the immobilized layer can be dependent on the initial solvent, changing the structure and the properties of the PNC significantly. In addition, we show that the outcome of the initial solvent effect becomes more effective at particle volume fractions where the immobile layers begin to interact.

DOI: 10.1103/PhysRevLett.123.167801

The incorporation of nanoparticles into a polymer matrix, thus creating polymer nanocomposites (PNCs), is regarded as a general strategy to enhance the physical properties of neat polymers [1–4]. However, the intrinsic incompatibility between nanoparticles and polymers requires the effective control of polymer-nanoparticle interactions at the interface. Polymers can be chemically grafted or physically adsorbed onto the particle surface, creating an immobilized layer, which is believed to control the resulting structures and properties of PNCs [5–9]. Many attempts have been made, therefore, to develop a stable immobilized layer by changing the chemical structure of particles or polymers and to characterize governing parameters such as grafting or adsorption density, the sizes of the polymers or particles, and their compositions [10–19].

A few studies, however, have reported on nonequilibrium effects present during the processing of PNCs [4,20–24]. While PNC production involves complicated yet dynamic processes such as initial dispersion in solvents, mixing with polymers, solvent evaporation, and drying, the relaxation time of polymers in the presence of nanoparticles may significantly increase, suggesting that the polymers and particles may not reach their equilibrium structures in experimentally accessible processing times, becoming kinetically trapped [25,26].

In this Letter, we report that when the initial dispersing solvent is varied, PNCs may not reach their equilibrium state, resulting in a dramatic change in particle dispersion, polymer dynamics, and rheological properties. We compose PNCs with poly(ethylene glycol) (PEG) and silica nanoparticles using either ethanol or water as casting solvents. Employing extensive small-angle x-ray scattering (SAXS), NMR free induction decay (FID), double-quantum (DQ), and rheometry experiments, we find that the initial solvent influences (i) the initial and final particle microstructure, (ii) the dynamics of the immobilized layers, and (iii) the resulting physical properties of the PNCs, even though the solvent was thoroughly evaporated and thus not present in the final state of the PNCs.

Silica nanoparticles 37 nm in size [27] were dispersed in either ethanol or water and vigorously mixed with PEG of varying molecular weights (MWs) (0.4 and 20 kg/mol) and particle volume fractions ($\phi_c = 0.05$–0.5). The PNCs were prepared by quickly evaporating the solvent in a vacuum oven at 70 °C. All experiments were performed at 75 °C. The samples are labeled as "initial solvent-PEG MW-ϕ_c." For example, EtOH-PEG0.4k-0.3 indicates a PNC composed of 30 vol% of silica particles in PEG 0.4 kg/mol, initially dispersed in ethanol.

The detailed microstructures of particle dispersion were explored with SAXS. The scattered intensity at wave vector q, $I(q)$, is given as $I(q) \sim \phi_c P(q) S(q, \phi_c)$, where $P(q)$ and $S(q, \phi_c)$ are the particle form and structure factors, respectively. The structure factor contains information about the interparticle correlations and can be extracted by dividing $I(q)$ by the $I(q)$ at the dilute limit (see Ref. [28] and Fig. S3

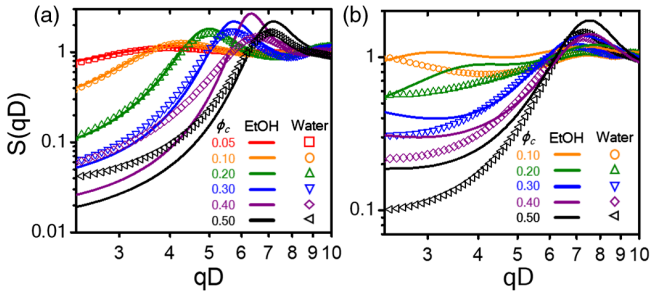

FIG. 1. The structure factors $S(qD)$ of silica nanoparticles in PNCs are plotted with qD where D is particle diameter, for PEG MWs of (a) 0.4 kg/mol and (b) 20 kg/mol. The solid curves and open symbols represent EtOH– and water-started PNCs, respectively.

in the Supplemental Material [29]). Figure 1 shows the extracted structure factor of PNCs in PEG 0.4 and PEG 20 kg/mol with varying ϕ_c.

The SAXS results of unentangled low-MW 0.4 kg/mol are shown in Fig. 1(a). The systems become less compressible, and the degree of particle ordering increases with increasing ϕ_c in systems started in both solvents. We also find little difference in the positions of the peaks, $q*D$, depending on the initial solvent and that the $q*D$ continuously increase with increasing ϕ_c for both systems, implying that the average center-to-center distances of the particles decreases with increasing ϕ_c [34].

However, clear differences are found between systems started in the two solvents, especially at high ϕ_c. The peak heights $S(q*D)$ of the EtOH-started systems are higher than those of water-started systems, implying that the nanoparticles are ordered better in the EtOH systems. Second, the PNCs of the EtOH-started systems are less compressible and more repulsive, represented by the $S(qD)$ value at the low $qD = 2.3$. For low-MW PNCs, EtOH as the initial solvent provides better dispersion and stability of nanoparticles with stronger repulsive interaction than water (Fig. S4).

For entangled high-MW PEG 20 kg/mol shown in Fig. 1(b), the initial solvent-dependent structures vary with ϕ_c. At $\phi_c = 0.1$–0.2, two peaks develop for EtOH-PEG20k-0.1 and 0.2, implying the formation of multi-length-scale structures; the peak around 0.021 $Å^{-1}$ of q indicates that the particles are almost in contact ($q*D \sim 7$), and an additional peak ($q**$) is found at lower q from the cluster–cluster interactions. In addition, the decrease of $S(q)$ at a low-q limit with a scaling behavior of $q** \sim \phi_c^{1/3}$ (Fig. S4) implies that the aggregated clusters were repulsive [35]. In comparison, water-PEG20k-0.1 and 0.2 shows only one correlation peak originating from loosely packed networked nanoparticle systems, showing upturns at low q with negative slopes of 1.6 and 0.8 [36].

However, when ϕ_c increases to 0.3–0.5, where particles are close to neighboring particles, low-q upturns are found with the EtOH-started PNCs, with negative slopes of 1.14, 1.26, and 0.62, which suggests the formation of fractal-like aggregates in the EtOH-started systems [36]. However, suppressed upturns from the water-started PNCs imply less sturdy networks of nanoparticles, with reduced aggregation dimension compared to EtOH-started PNCs. Additional evidence that stronger particle networks form in the EtOH-started PNCs is found in the higher $q*$ ($q*D \sim 7$) and higher $S(q*D \sim 7)$ of the EtOH-started PNCs; this result implies that particles are more tightly packed in the EtOH-started PNCs, with a shorter interparticle distance and stronger coherence between the particles.

Because the solvents quickly evaporate during the production of PNCs and thus are not present in the final state (Fig. S2), the significantly different microstructures and dispersion states of the nanoparticles depending on the initial solvents suggest that an initial solvent-driven nonequilibrium effect is present, which could originate from different solvent–particle and solvent–polymer interactions in the initial dispersion states. The apparent difference in evaporation rates between EtOH and water may affect the nanoparticle dispersions [37–39] in the PNCs. To confirm the effect of evaporation rate, we let both solvents evaporate at similar rates by changing the temperature and pressure of the vacuum oven (Fig. S6). However, solvent-dependent differences in particle microstructure consistently appear, suggesting that the initial solvent–driven nonequilibrium effect does not originate from differences in evaporation rate but is intrinsically present.

Because the mobility and the conformation of polymer chains are generally restricted at interfaces [7,40–42], a severe nonequilibrium effect is thought to originate from the change of polymer dynamics near nanoparticle surfaces. We employ the ^{1}H NMR FID measurements, as it is a well-established technique quantifying the domains of different polymer mobilities [30,31,43–45]. Figure 2(a) shows the FID signals of EtOH-PEG0.4k-0.5 and water-PEG0.4k-0.5. Because of favorable interactions between nanoparticles and polymers, the mobility of the polymers significantly decreases near the particle surface. Accordingly, the FID signal decays with more than two relaxation times due to a mobility gradient as a function of distance from the particle surface [3]. The FID of EtOH-PEG0.4k-0.5 decays much faster than that of water-PEG0.4k-0.5. Consistently, the amplitude of the Gaussian decay of a double-quantum (DQ)-filtered FID, which selectively reveals confined components with very short T_2 [30,31,46], is higher in EtOH-PEG0.4k-0.5. Additionally, a magic and polarization echo (MAPE)-filtered NMR signal isolates the mobile component [30,31,44,46]. The decaying behaviors of the MAPE signal between two PNCs are very similar to each other, but the normalized intensity of EtOH-0.4k-0.5 is smaller than that of water-PEG0.4k-0.5. Such differences in the normalized intensity and decaying behavior of intensity of unfiltered and filtered NMR experiments depending on the initial solvent are consistently observed for all other PNCs. Thus,

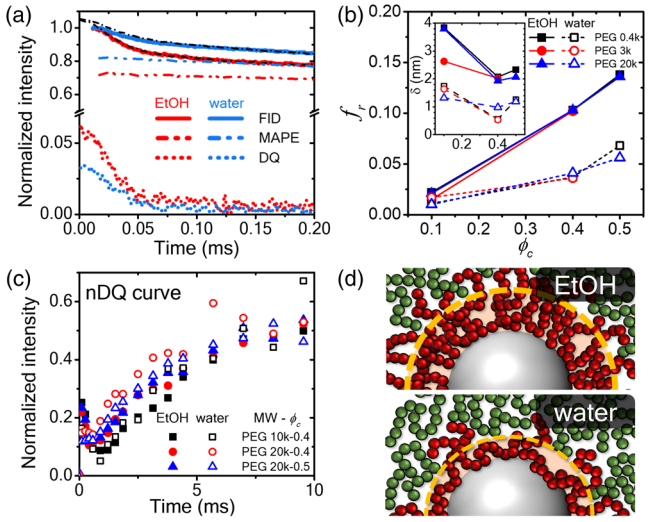

FIG. 2. (a) Normalized FID, magic-sandwich echo (MSE), MAPE-, and DQ-filtered intensities of EtOH-PEG0.4k-0.5 and water-PEG0.4k-0.5. The black dashed dot lines are MSE-filtered FID. (b) The calculated strongly immobilized polymer fractions as a function of ϕ_c in ethanol- and water-started PNCs with closed and open symbols, respectively. (Inset) Calculated layer thickness δ. (c) nDQ curve. (d) Schematic illustrations of the nanoparticle surface in PNCs. Red and green chains are adsorbed and bulk polymers distinguished by the yellow dashed line.

the EtOH-started PNCs contain more confined polymers than the water-started PNCs at the given composition.

To quantify each polymer fraction in terms of mobility, the given FID intensities are fitted to the Kohlrausch–Williams–Watts (KWW) equation [30], assuming three components of strongly immobilized, intermediate, and mobility polymer dynamics, defined as $I = A\{f_r \exp[-(t/\tau_r)^{b_r}] + f_i \exp[-(t/\tau_i)^{b_i}] + f_m \exp[-(t/\tau_m)^{b_m}]\}$, where A is a scaling factor, τ is the T_2 relaxation time, b the stretching exponent, f the fraction of polymer segments with each mobility, with subscripts r, i, and m representing the strongly immobilized [47], intermediate, and mobile parts, respectively. The intermediate polymer mobility needs to be included because fitting with two components results in poor quality, suggesting that the polymer mobility gradually changes from the interface to the bulk as previously confirmed [30]. The DQ- and MAPE-filtered NMR signals are used to acquire the shape parameters for the strongly immobilized (τ_r, b_r) and mobile (τ_m, b_m) parts of the polymers. With fixed values of τ_r, b_r, τ_m, and b_m, fitting the FID by the three-component KWW model to obtain just the fractions as well as τ_i and b_i enables us to quantify each segment fraction with different mobilities (f_r, f_i, f_m). The detailed fitting results and procedures are found in Table S1 in Ref. [29] and Refs. [30,31,47], respectively.

Figure 2(b) shows the corresponding fitting results. The fraction of strongly immobilized polymers increases with increasing ϕ_c as increasing ϕ_c provides for a larger surface area of particles for polymers to be adsorbed. However, the fraction of strongly immobilized parts is independent of the polymer MW at fixed ϕ_c, consistent with previous studies [30]. The layer thicknesses are given in the inset, estimated from the immobile fraction using the Eq. (2) in Ref. [47]. The most intriguing result is that all EtOH-started PNCs have strongly immobilized fractions that are 2 times higher than those of water-started PNCs, despite having the same compositions. When the dispersing solvent is ethanol, a larger number of polymer segments is adsorbed, creating thicker immobilized layers on the nanoparticle surfaces, as illustrated in Fig. 2(d).

Consistent results are also found by fitting the SAXS intensities of the PEG 0.4k PNCs with the Percus-Yevick (PY) prediction based on a hard-sphere model [32] (Fig. S5 in Ref. [29]). The fitting with PY generates the effective ϕ_c and the radii of the particles, which are higher than the actual ϕ_c and the radii of the particles because of the adsorbed polymer layers. We find that EtOH-started PNCs have larger values than the water-started PNCs at the given ϕ_c, demonstrating again the formation of thicker immobilized layers for the EtOH-started PNCs.

Possible nonpolymeric contributions to the FID signal such as the Si–O–Et units that can be formed during drying [33], and Si–OH, are excluded as silica particles in pure solvent treated identically as drying of PNCs does not show any noticeable DQ-filtered FID signals (see Fig. S7 for details).

Using multiple-quantum (MQ) NMR experiments, we investigate the effect of the initial solvent on polymer dynamics in the bulk mobile phase where an elastic network built from bridging and entanglements can be present [48]. MQ NMR experiments characterize the anisotropic motion of mobile polymers arising in an elastic network by probing the long-time behavior of angle-dependent spin–spin dipolar couplings, which leads to measurable residual dipolar couplings (RDCs) in the case of end-fixed chains. Raw data treatment involves the removal of relaxation effects for the measured DQ buildup, leading to normalized DQ (nDQ) curves. The results of the PNCs at high ϕ_c in high MW are presented in Fig. 2(c). The important finding is that the general shapes and initial increase of the nDQ curves, reflecting finite RDCs, do not differ significantly as the initial solvents change with identical compositions of PNCs. The resulting networklike fractions for varying initial solvents are provided in Table S2 in Ref. [29]. From there, we can conclude that the immobilized polymer fractions mainly contribute to creating different particle microstructures that dominate the rheological properties.

It is striking that the amount of immobilized polymer at the interface depends on the initial solvent, even though solvent molecules completely evaporate (Fig. S2) and the production of the PNCs is performed above T_m to ensure sufficient mobility. While water is known to be a good solvent [49] and exhibits temperature-dependent solvent quality for PEG, a previous study showed that the degree of

PEG adsorption decreases significantly with temperature [50]. Thus, when the solvent quality is varied from water to ethanol, a more favorable PEG–silica interaction comes into play, resulting in a thicker immobilized layer in ethanol. The different immobile layer thicknesses even remain effective in PNCs, owing to the kinetically trapped chains with rapid solvent evaporation [20].

Because the immobilized layer is believed to be critical for determining the microstructure and the resulting physical properties [51], consistent variations in the immobilized layer depending on the initial dispersing solvent may trigger substantial changes in the rheological properties. Figures 3(a) and 3(b) compare the elastic (G') and viscous (G'') moduli of the PNC in PEG 0.4k from strain sweep experiments depending on the initial solvent. No noticeable difference is found up to $\phi_c \approx 0.3$ as they remain liquidlike. However, at $\phi_c \approx 0.4$, the G' and G'' of water-PEG0.4k-0.4 is substantially higher than the G' and G'' of EtOH-PEG0.4k-0.4. In addition, water-PEG0.4k-0.4 exhibits glassy behavior, showing initial plateaus at low strain and power-law decay at high strain ($G' \sim \gamma^{-1.8}$, $G'' \sim \gamma^{-0.8}$)

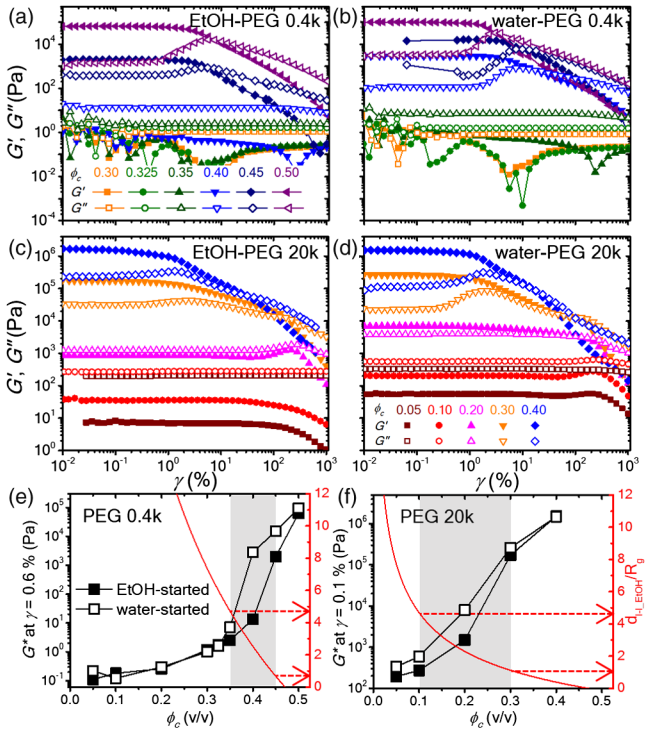

FIG. 3. Storage and loss modulus, G' and G'', of PNCs as a function of complex shear strain γ at 1 Hz, for PEG 0.4 kg/mol, (a) EtOH- and (b) water-started PNCs. The results of PEG 0.4 k PNCs at ϕ_c lower than 0.3 are given in Fig. S10. For PEG 20 kg/mol, (c) EtOH- and (d) water-started PNCs. The complex shear modulus G^* of PNCs are compared for different initial solvents with (e) PEG 0.4 kg/mol at $\gamma = 0.6\%$ and (f) PEG 20 kg/mol at $\gamma = 0.1\%$. The normalized layer-to-layer distances with R_g are drawn with ϕ_c assuming random close packing, based on the EtOH-started samples. A complementary frequency sweep experiment is provided in Fig. S9.

[8,52]. The nanoparticles are less stable in the water-started PNCs because of the weaker steric repulsion with the thinner immobilized layer, resulting in large variation in the local density of particles; nanoparticles can be easily vitrified, forming a local colloidal glass region [52]. Thus, the decreased particle stability with the thinner immobilized layer results in a remarkable increase in the shear modulus by a factor of 10^4. This result suggests that the rheological properties of PNC are not solely dependent on individual particle stability, but rather, they rely on overall structures at multiple length scales.

When the nanoparticles are dispersed in high-MW PEG20k, as shown in Figs. 3(c) and 3(d), the effect of the initial dispersing solvent changes more dramatically with changing ϕ_c. When ϕ_c is low (0.05–0.2), the thicker immobilized layer created from the EtOH-started system helps structure nanoparticles as small clusters. Because the small clusters do not create a percolating rigid network throughout the system and clusters are mutually repulsive, the system remains liquidlike [35], and thus the shear moduli of the EtOH-started system are much lower than those of the water-started system. The G' and G'' moduli of EtOH-PEG20k-0.2 decrease after a yielding at around $\gamma = 170\%$, attributed to the disruption of particle clusters. In contrast, poorly dispersed nanoparticles in water-PEG20k-0.2 have stronger interparticle attraction, forming a weak network with $G' > G''$, and showing a yielding at high γ similar to that of water-0.4k-0.4 [36].

When the ϕ_c is as high as 0.3 in PEG20k, nanoparticles from both the EtOH- and water-started systems form a particle network with $G' > G''$, with a significantly increased shear modulus [53]. As the shear strain increases, the nanoparticles experience network-to-cluster and cluster-to-individual particle transitions exhibiting two yield strains. Although the nanoparticles started in both solvent systems show similar behavior, the modulus of the water-started PNC drops more rapidly at each yield strain. In addition, the crossover strain of the solid-to-liquid transition is higher in ethanol, presumably due to the thicker immobilized layer creating a sturdier network than in the water-started systems.

The initial solvent-driven nonequilibrium effect has a remarkable influence on the properties of PNCs; however, the outcome of the nonequilibrium effect may vary depending on ϕ_c. Figures 3(e) and 3(f) compare the differences in complex shear modulus G^* at a constant strain. The differences in G^* for different solvents increase with increasing ϕ_c, and these differences become significant near $\phi_c = 0.35$–0.45 and 0.10–0.30 for PEG 0.4k and 20k, respectively. Although the range of critical ϕ_c varies with polymer MW, the layer-to-layer spacing normalized to the radius of polymer gyration, d_{l-l}/R_g, in the critical ϕ_c range is surprisingly close to around 1–$5R_g$ for both PEG 0.4k and 20k. At higher ϕ_c, the difference in G^* rapidly decreases as immobile layers begin to overlap.

These findings suggest that the initial solvent-driven nonequilibrium effect can be critical when the immobile layers are close enough to interact with one another via the associated dangling chains. Despite large particle spacing exceeding R_g in the critical ϕ_c range, the confinement effect can be effective in the case of nonequilibrated polymer adsorption [54]. These implications are obviously crucial to designing ideal processing conditions for PNCs.

Taken together, we find that the initial dispersing solvent has a significant effect on PNCs even after complete solvent evaporation, leading to significantly different interfacial properties of the PNCs. An initial solvent-driven nonequilibrium effect determines the structure and dynamics of interfacial layers, changing the thickness of the immobilized layer, the overall particle dispersions, and the rheological properties. Schematic illustrations of the initial solvent effect on the microstructure are depicted in Fig. 4. When the polymer chain length is short, the thicker immobilized layer from the EtOH-started system imparts greater dispersion stability to nanoparticles with sterically more repulsive interactions. The nanoparticles in a water-started system are poorly ordered, resulting in vitrification that increases the shear modulus of the PNC.

When the chain length of the polymer is long enough to be entangled, the thicker immobilized layer at low ϕ_c in EtOH-started PNCs creates small repulsive clusters, whereas the thinner immobilized layer in water-started PNCs forms loosely connected aggregates. However, at high ϕ_c, PNCs from both solvents behave qualitatively similar, forming networks in which thicker immobilized layers facilitate tight packing of the nanoparticles. The adsorbed entangled polymers with loop and tail conformations [18] enable (possibly entanglement-mediated) bridging between particles, which can occur more easily with the increased thickness of the adsorption layer [36,55]. Thus, particles in EtOH-started PNCs are more aggregated with a high fractal dimension.

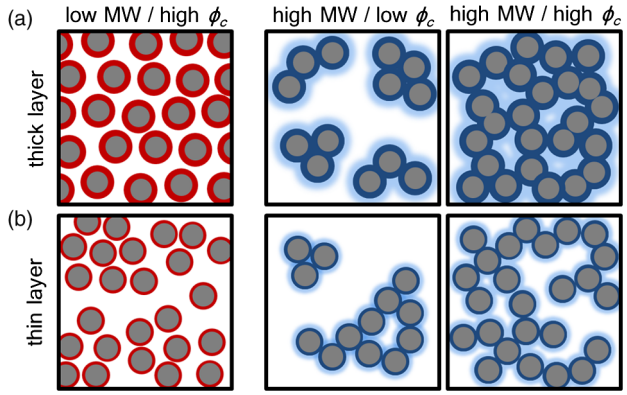

FIG. 4. Schematic illustration of nanoparticle dispersions in (a) EtOH-started (thick layer) and (b) water-started (thin layer) PNCs at low and high ϕ_c. The strongly immobilized polymers are colored in solid red and blue for low and high MW, respectively, and the faded blue is used to represent loops and tails of the immobilized layers.

Although solvent quality is well known to alter the interfacial properties of nanoparticles, creating thicker or thinner immobilized layers in polymer solutions, it is noteworthy that a solvent-driven nonequilibrium effect is present in PNCs even after thorough solvent evaporation. The limited mobility of nanoparticles and polymers during solvent evaporation leads to kinetic trapping. The infinitesimal differences in immobilized layer thickness on a nanometer scale can thus change the final structure and rheological properties of PNCs substantially. We emphasize that an in-depth understanding of nonequilibrium effects is both important and relevant, as are delicate variations in the chemistry or compositions in PNCs.

This work was supported by the Research Program through the National Research Foundation of Korea (NRF) funded by the Ministry of Education (Grants No. NRF-2015K2A9A2A18065964 and No. NRF-2018R1A2B6008319) and the Deutsche Forschungsgemeinschaft (German Research Foundation, DFG, Grant No. SA982/13-1, and Project No. 316439043). SAXS measurements at the PLS-II 6D beamline of the Pohang Accelerator Laboratory (PAL) were supported in part by UCRF, MSIP, and POSTECH.

*soyounkim@unist.ac.kr
†kay.saalwaechter@physik.uni-halle.de

[1] T. Kashiwagi, F. Du, J. F. Douglas, K. I. Winey, R. H. Harris, Jr., and J. R. Shields, Nat. Mater. **4**, 928 (2005).
[2] A. C. Balazs, T. Emrick, and T. P. Russell, Science **314**, 1107 (2006).
[3] A. Papon, H. Montes, M. Hanafi, F. Lequeux, L. Guy, and K. Saalwächter, Phys. Rev. Lett. **108**, 065702 (2012).
[4] S. K. Kumar, V. Ganesan, and R. A. Riggleman, J. Chem. Phys. **147**, 020901 (2017).
[5] G. Tsagaropoulos and A. Eisenberg, Macromolecules **28**, 6067 (1995).
[6] P. Rittigstein and J. M. Torkelson, J. Polym. Sci. B **44**, 2935 (2006).
[7] A. P. Holt *et al.*, ACS Nano **10**, 6843 (2016).
[8] N. K. Kwon, H. Kim, I. K. Han, T. J. Shin, H.-W. Lee, J. Park, and S. Y. Kim, ACS Macro Lett. **7**, 962 (2018).
[9] S. Yang, M. Hassan, and P. Akcora, J. Polym. Sci. B **57**, 9 (2019).
[10] E. Hershkovits, A. Tannenbaum, and R. Tannenbaum, J. Phys. Chem. C **111**, 12369 (2007).
[11] S. Y. Kim, K. S. Schweizer, and C. F. Zukoski, Phys. Rev. Lett. **107**, 225504 (2011).
[12] S. K. Kumar, N. Jouault, B. Benicewicz, and T. Neely, Macromolecules **46**, 3199 (2013).
[13] N. Jouault, J. F. Moll, D. Meng, K. Windsor, S. Ramcharan, C. Kearney, and S. K. Kumar, ACS Macro Lett. **2**, 371 (2013).
[14] M. Füllbrandt, P. J. Purohit, and A. Schönhals, Macromolecules **46**, 4626 (2013).

[15] N. Jouault, D. Lee, D. Zhao, and S. K. Kumar, Adv. Mater. **26**, 4031 (2014).
[16] A. P. Holt, P. J. Griffin, V. Bocharova, A. L. Agapov, A. E. Imel, M. D. Dadmun, J. R. Sangoro, and A. P. Sokolov, Macromolecules **47**, 1837 (2014).
[17] S. Gong, Q. Chen, J. F. Moll, S. K. Kumar, and R. H. Colby, ACS Macro Lett. **3**, 773 (2014).
[18] S. Cheng *et al.*, Phys. Rev. Lett. **116**, 038302 (2016).
[19] H. Emamy, S. K. Kumar, and F. W. Starr, Phys. Rev. Lett. **121**, 207801 (2018).
[20] N. Jouault, D. Zhao, and S. K. Kumar, Macromolecules **47**, 5246 (2014).
[21] P. Lepcio, F. Ondreas, K. Zarybnicka, M. Zboncak, O. Caha, and J. Jancar, Soft Matter **14**, 2094 (2018).
[22] M. J. Park, K. Char, J. Park, and T. Hyeon, Langmuir **22**, 1375 (2006).
[23] A. K. Kota, B. H. Cipriano, M. K. Duesterberg, A. L. Gershon, D. Powell, S. R. Raghavan, and H. A. Bruck, Macromolecules **40**, 7400 (2007).
[24] A. J. Moulé and K. Meerholz, Adv. Funct. Mater. **19**, 3028 (2009).
[25] S. Napolitano and M. Wübbenhorst, Nat. Commun. **2**, 260 (2011).
[26] S. Chandran *et al.*, Macromolecules **52**, 7146 (2019).
[27] W. Stöber, A. Fink, and E. Bohn, J. Colloid Interface Sci. **26**, 62 (1968).
[28] S. Y. Kim, L. M. Hall, K. S. Schweizer, and C. F. Zukoski, Macromolecules **43**, 10123 (2010).
[29] See Supplemental Material at http://link.aps.org/supplemental/10.1103/PhysRevLett.123.167801, which includes Refs. [27,30–33], for detailed description of experiments, additional data, and analysis.
[30] S. Y. Kim, H. W. Meyer, K. Saalwächter, and C. F. Zukoski, Macromolecules **45**, 4225 (2012).
[31] K. Schäler, M. Roos, P. Micke, Y. Golitsyn, A. Seidlitz, T. Thurn-Albrecht, H. Schneider, G. Hempel, and K. Saalwächter, Solid State Nucl. Magn. Reson. **72**, 50 (2015).
[32] J. K. Percus and G. J. Yevick, Phys. Rev. **110**, 1 (1958).
[33] K. Saalwächter, M. Krause, and W. Gronski, Chem. Mater. **16**, 4071 (2004).
[34] B. J. Anderson and C. F. Zukoski, Macromolecules **41**, 9326 (2008).
[35] N. Jouault, P. Vallat, F. Dalmas, S. Said, J. Jestin, and F. Boué, Macromolecules **42**, 2031 (2009).
[36] B. J. Anderson and C. F. Zukoski, Macromolecules **42**, 8370 (2009).
[37] K. E. Strawhecker, S. K. Kumar, J. F. Douglas, and A. Karim, Macromolecules **34**, 4669 (2001).
[38] S. Cheng and G. S. Grest, ACS Macro Lett. **5**, 694 (2016).
[39] H. Chao, J. Koski, and R. A. Riggleman, Soft Matter **13**, 239 (2017).
[40] S. Kaufman, W. P. Slichter, and D. D. Davis, J. Polym. Sci., A-2, Polym. Phys. **9**, 829 (1971).
[41] A. Papon, H. Montes, F. Lequeux, J. Oberdisse, K. Saalwächter, and L. Guy, Soft Matter **8**, 4090 (2012).
[42] S. Cheng, S. Mirigian, J.-M. Y. Carrillo, V. Bocharova, B. G. Sumpter, K. S. Schweizer, and A. P. Sokolov, J. Chem. Phys. **143**, 194704 (2015).
[43] V. M. Litvinov, H. Barthel, and J. Weis, Macromolecules **35**, 4356 (2002).
[44] A. Papon, K. Saalwächter, K. Schäler, L. Guy, F. Lequeux, and H. Montes, Macromolecules **44**, 913 (2011).
[45] S. Y. Kim and C. F. Zukoski, Macromolecules **46**, 6634 (2013).
[46] M. Mauri, Y. Thomann, H. Schneider, and K. Saalwächter, Solid State Nucl. Magn. Reson. **34**, 125 (2008).
[47] Y. Golitsyn, G. J. Schneider, and K. Saalwächter, J. Chem. Phys. **146**, 203303 (2017).
[48] K. Saalwächter, Prog. Nucl. Magn. Reson. Spectrosc. **51**, 1 (2007).
[49] R. Kjellander and E. Florin, J. Chem. Soc., Faraday Trans. 1 **77**, 2053 (1981).
[50] N. K. Kwon, C. S. Park, C. H. Lee, Y. S. Kim, C. F. Zukoski, and S. Y. Kim, Macromolecules **49**, 2307 (2016).
[51] A. Mujtaba, M. Keller, S. Ilisch, H.-J. Radusch, M. Beiner, T. Thurn-Albrecht, and K. Saalwächter, ACS Macro Lett. **3**, 481 (2014).
[52] B. J. Anderson and C. F. Zukoski, J. Phys. Condens. Matter **21**, 285102 (2009).
[53] G. P. Baeza, C. Dessi, S. Costanzo, D. Zhao, S. Gong, A. Alegria, R. H. Colby, M. Rubinstein, D. Vlassopoulos, and S. K. Kumar, Nat. Commun. **7**, 11368 (2016).
[54] D. N. Simavilla, W. Huang, C. Housmans, M. Sferrazza, and S. Napolitano, ACS Cent. Sci. **4**, 755 (2018).
[55] M. Kawaguchi, R. Naka, M. Imai, and T. Kato, Langmuir **11**, 4323 (1995).